Fibers and Polymers 2020, Vol.21, No.1, 127-137
DOI 10.1007/s12221-020-9346-5

ISSN 1229-9197 (print version)
ISSN 1875-0052 (electronic version)

Role of Carbon Black for Enhancing the Mechanical Properties of Short Aramid Fiber Reinforced Ethylene-Acrylic Rubber

Yoonjae Seong, Shibulal Gopi Sathi*, Jongho Park, In-Seok Park, and Changwoon Nah*

Haptic Polymer Composite Research Team, Department of Polymer-Nano Science and Technology, Jeonbuk National University, Jeonju 54896, Korea

(Received April 8, 2019; Revised July 1, 2019; Accepted July 4, 2019)

Abstract: Composites based on ethylene-acrylic rubber and 1 mm short aramid fibers (AF) were developed by varying the fiber content from 3 to 40 phr. At 10 phr short fiber loading, the tensile modulus (10 % modulus) of the neat matrix was around 11 times increased. However, its breaking elongation was decreased from 408 to 58 %. This drastic reduction in the breaking elongation even at a 10 phr fiber loading leads to a brittle failure with inferior toughness. The tensile-fractured surface of the fiber-filled composite showed an intact matrix with no plastic deformation during fiber pulled-out. To solve this problem, carbon black (CB) was used as a toughening agent. Surprisingly, the addition of 20 phr CB onto a 10 phr AF-filled composite enhanced its 10 % modulus in the longitudinal direction by 70 % and also enhanced its breaking elongation from 58 to 351 %. From the morphological analysis, it has been presumed that the addition of CB enhanced the friction between the fiber and the matrix at a very low strain and also facilitate the matrix for a plastic deformation at a higher strain. This enhanced friction between the fiber and the matrix is considered as the improved low strain modulus and the subsequent plastic deformation at a higher strain is responsible for the improved toughness.

Keywords: Rubber, Short fiber, Composite, Mechanical properties, Morphology

Introduction

For many years, short fibers are widely used as reinforcing fillers in elastomers, plastics and thermoplastic elastomers. In comparison with the reinforcing fillers like carbon black or silica, short fibers can provide a high degree of low strain modulus (stiffness) together with good dimensional and thermal properties to the polymer matrix at a low fiber content. Unlike continuous fiber reinforced polymers, the short fiber reinforced one can be processed by all the conventional manufacturing techniques such as injection molding, extrusion, and casting. Moreover, short fiber reinforced polymers can exhibit specific fiber orientation and hence can show anisotropy in their tensile properties, such as tensile strength, tensile modulus, tensile hysteresis and tear resistance [1-6]. As far as the short fiber reinforcement of polymers is concerned, aramid fiber (AF) is one of the potential candidates to improve the mechanical and thermal properties. Earlier many researchers have reported various studies with different kinds of short AFs on different types of elastomeric matrixes [7-23]. For instance, Wennekes *et al*. explored various aspects of the adhesion between resorcinol formaldehyde latex (RFL) treated Twaron AF on natural rubber (NR) and styrene-butadiene rubber (SBR) and a model carcass master batch NR/SBR blend [7-9]. Praveen *et al*. investigated the effect of nano-clay on the mechanical properties of short AF-filled SBR composite and claimed that nano-clay has a tendency to adhere over the short fiber surface which brings a marked improvement in elongation of the composite [10]. Shirazi *et al*. explored the reinforcing effect of RFL coated Twaron short AF on NR and ethylene-propylene-diene-Monomer (EPDM) [11-13]. Hintze *et al*. reported the influence of fiber type and coating on the composite properties of EPDM compounds reinforced with short AFs. They have also reported the influence of processing techniques on the properties of short Twaron AF reinforced EPDM [14,15]. Based on the earlier research work, it has been identified that one of the limiting factors for the widespread use of short AFs in the rubber matrix is its poor adhesion with the rubber matrix [23]. As a result, it cannot establish a strong fiber-matrix interfacial adhesion, which ultimately leads to poor toughness of the composite. Moreover, poor fiber dispersion in the rubber matrix even at a very low loading causing aggregated fiber lumps in the matrix. These aggregated fibers act as stress concentrated areas during tensile deformation resulting in a brittle failure with poor elongation and toughness.

It is well known that carbon black(CB) can reinforce almost all the rubbers and can impart a certain level of both low and high strain modulus without compromising the elongation at break or toughness of the composites [24]. However, the modulus (stiffness) offered by the reinforcement of carbon black is much lower than the short fiber reinforced one. Therefore, in the present work, we explored the reinforcing effects of a combination of short AF and CB on the mechanical, dynamic mechanical and morphological properties of an ethylene acrylic elastomer.

*Corresponding author: gslal2009@gmail.com
*Corresponding author: cnah@jbnu.ac.kr

Experimental

Materials

Ethylene-acrylic rubber (Vamac DP, Mooney viscosity ML (1+4) of 22 at 100 °C, purchased from DuPont, USA) was used as the base elastomer. The peroxide alfa, alfa' Di (t-butylperoxy)diisopropylbenzene (Luperox F40P-SP2 E) with a purity of 38-42 % (purchased from Arkema, 21, Gukhoe-daero, Seoul, South Korea) was used as the curing agent. Triallyl isocyanurate (TAIC) obtained from TCI, Sinmonk, South Korea was used as the co-agent agent for the peroxide vulcanization. The fillers such as short aramid fiber and carbon black (Purex®HS 45) were obtained respectively from Kolon Industries, South Korea and Orion Engineered Carbon GmbH, Germany. The detailed specifications of aramid fiber is given in Table 1.

Preparation of the Composites

The formulations used for the preparations of composites are displayed in Table 2. All the composites were prepared by mechanical mixing of the components using an internal mixer (Banbury-type mixer, Nam Yang Corporation, South Korea) at a temperature of 50 °C with a rotor speed of 50 rpm for 6 minutes. The neat rubber was masticated for 2 minute. To this, the short fiber (or carbon black) were added and the mixing was continued for 2 minutes. The peroxide and co-agent: Triallyl isocyanurate (TAIC) were then added and the mixing was continued at the same rpm for 2 more minutes. After the mixing, the compound was discharged and forced the fibre-filled rubber compound using a two-roll mill with a tight nip gap to orient the fibres in the mill direction. The specifically oriented fibre compound is then molded into a 2 mm sheet at 180 °C as per the respective cure time using a compression molding press (CMV 50H-15-CLPX, CARVER®, USA) at a constant pressure of 25 ton.

Table 1. Technical specification of the Aramid short fiber

Properties	Values
Color	Gold
Specific gravity	1.4
Coating	RFL*
Average fiber length (mm)	1
Diameter (μm)	11-12
Average aspect ratio (L/D ratio)	87
Young's modulus (GPa)	94
Tensile strength (GPa)	2.9
Elongation at break (%)	3.3

*Resorcinol Formaldehyde Latex.

Table 2. Formulations of the mixes in phr (Parts per hundred rubbers)

Sample designation*	Rubber	Peroxide	Co-agent	Aramid fiber	Carbon black
Neat	100	2	1	-	-
AF_3	100	2	1	3	-
AF_5	100	2	1	5	-
AF_{10}	100	2	1	10	-
AF_{20}	100	2	1	20	-
AF_{30}	100	2	1	30	-
AF_{40}	100	2	1	40	-
CB_{10}	100	2	1	-	10
CB_{20}	100	2	1	-	20
CB_{30}	100	2	1	-	30
CB_{40}	100	2	1	-	40
AF_{10}+CB_{20}	100	2	1	10	20

*AF indicates aramid fiber, CB indicates carbon black and the subscript number is its content in phr.

Characterization of the Composites

Cure Characteristics

The most important technical parameters in a vulcanization process such as the maximum torque: M_H, minimum torque: M_L, the difference between maximum and minimum torque: DM, scorch time: T_{S2}, optimum cure time: T_{90} (the time required for the torque to reach 90 % of the maximum torque) of the rubber compounds were determined from the cure curves generated by an oscillating disk rheometer (ODR, Alpha Technologies, USA) at 180 °C as per ASTM D 2084.

Mechanical Properties

Tensile Testing

The tensile test was carried out using LRX plus (Lloyd Instruments, UK) machine in accordance with the ASTM D-412. Dumbbell-shaped specimens were prepared from the molded sheets of the samples and tested at a cross-head speed of 500 mm/min at room temperature. Six samples have been taken for each compound and their averages with standard deviations are reported.

Hardness Testing

Round shaped samples having a thickness of 6 mm and a diameter of 10 mm with smooth and uniform surface were used to measure the indentation hardness of the cured samples using a Shore A hardness tester (Asker, Kobunishi Keiki Co. Ltd.) as per ASTM D2240 specification. By applying a constant force without any disturbances for a specific time, indentations were made in the various positions. Ten readings were taken from different areas of the testing samples and the average value was estimated.

Dynamic Mechanical Analyses (DMA)

The dynamic mechanical analysis was conducted on a dynamic mechanical analyser (DMA, TA instrument Q 800). Samples having rectangular geometry (length, width, thickness) of size 20.0, 5.3, 1.0 mm were used in tension mode at an amplitude of 0.05 micro meter and a frequency of 10 Hz at a

heating rate of 3 °C/min from -60 ° to +100 °C.

Thermogravimetric Analysis (TGA)

TGA was also carried out using TA instrument (Q50, USA) to understand the thermal degradation behavior of the composites. Samples were heated from room temperature to 600 °C at a heating rate of 10 °C/min under nitrogen atmosphere.

Morphological Analyses

Tensile fractured samples of the composites were analysed using (Carl Zeiss, Supra 40 VP, Germany) field emission scanning electron microscope (FESEM). The atomic force microscopy, AFM (Bruker, RTESP-300) was used to characterize the smoothly cut surface of the fiber-filled composite in the presence and absence of CB under tapping mode. The resonance frequency of the tip was maintained between 260-280 kHz and the force constant was kept at 40 Nm^{-1}.

Results and Discussion

Cure Characteristics

Figure 1(a, b) represents the vulcanization behavior of acrylic rubber with different content of AF and CB at 180 °C for 30 min. Their respective cure characteristics are displayed in Table 3. Neat rubber showed a minimum torque value of almost zero. This may be due to the inability to offer any shearing resistance owing to the extremely low viscosity of the rubber at the vulcanization temperature (180 °C). As the time elapsed, the torque was found to increase to a maximum of 8.43 dNm. With the incorporation of 3 phr of short fiber, the M_L value was increased by around 60 %. As the fiber content rose to 40 phr, the M_L value was dramatically increased to about 7000 %. This dramatic increase in the M_L value might be due to the enhanced compound viscosity owing to the possibility of polar interaction between the acrylic rubber and the RFL treated AF as depicted in Scheme 1. The maximum torque for the fiber-filled compounds were also increased due to the enhanced compound viscosity together with polar interaction between the fiber and the rubber. It is important to note that the induction time (scorch time) and the time to optimum cure (T_{90}) gradually reduced as the fiber-content increased. This may be not due to increasing the cure rate, but probably due to better reinforcement and enhanced stiffness of the compounds with fiber-loading. On the contrary, the CB-filled acrylic rubber always showed lower values of M_L and M_H compared to the

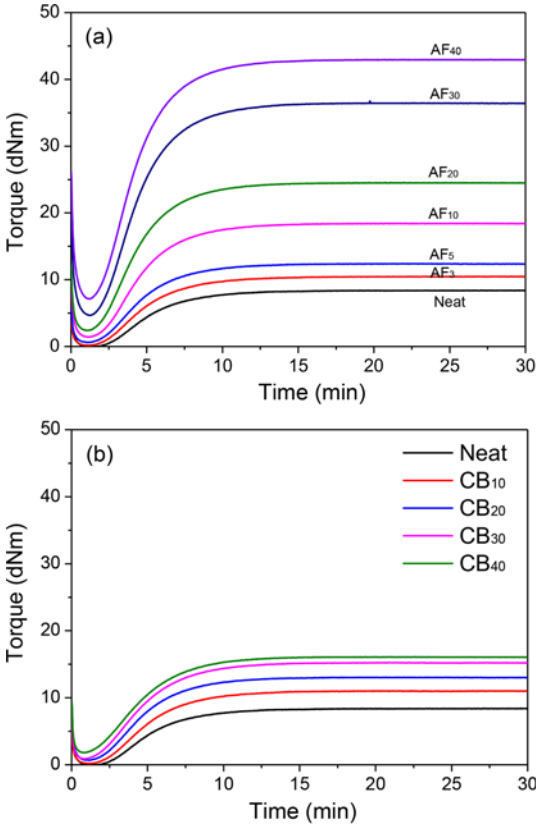

Figure 1. Cure curves of (a) short-aramid fiber-filled and (b) carbon black-filled acrylic rubber as a function of filler-loadings at 180 °C for 30 min.

Table 3. Cure characteristics of the composites with filler loadings

Compound	M_L (dNm)	M_H (dNm)	ΔM (dNm)	TS_2 (min)	T_{90} (min)
Neat	0.10	8.43	8.43	3.33	9.24
AF3	0.16	10.49	10.33	3.02	9.01
AF5	0.61	12.41	11.80	2:47	8.42
AF10	1.40	18.46	17.06	2.31	8.31
AF20	2.40	24.54	22.14	2.12	8.04
AF30	4.67	36.72	32.05	2.06	8.16
AF40	7.12	42.98	35.86	1.58	7.46
CB10	0.18	11.05	10.87	3.03	9.12
CB20	0.67	13.06	12.39	2.43	8.40
CB30	0.89	15.26	14.37	2.24	8.44
CB40	1.81	16.10	14.29	2.18	8.39

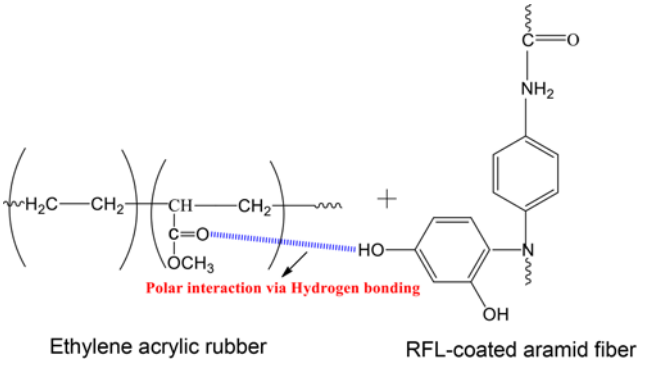

Scheme 1. Polar interaction between the ethylene-acrylic rubber and the RFL coated aramid short fiber via hydrogen bonding.

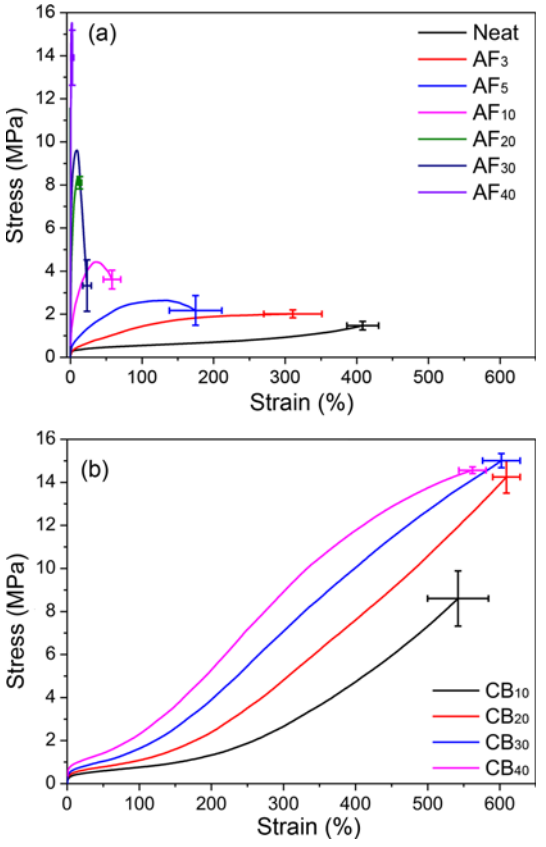

Figure 2. Stress-strain curves of (a) short-aramid fiber-filled acrylic rubber in the L direction and (b) carbon black-filled acrylic rubber as a function of filler-loadings.

AF-filled compounds. For instance, at 40 phr of AF loading, the M_L of neat acrylic rubber was increased from 0.1 to 7.12 dNm. Whereas, at the same loading, the CB-filled rubber compound showed an M_L value of just 1.81 dNm. This confirms that the higher ΔM during the vulcanization of AF-filled compound is partially due to the chemical interaction between the fiber and the matrix and partially due to the crosslinking torque. However, the ΔM generated by the CB-filled rubber compound is primarily due to the crosslinking reaction. Therefore the addition of CB does not significantly affected the Ts_2 and T_{90} values of the neat matrix.

Stress-strain Behavior and Tensile Properties

Represented in Figures 2(a, b) are the stress-strain behaviour of AF-filled compounds (in the longitudinal direction) and the CB-filled compounds as a function of filler loading. The mechanical properties such as tensile strength (TS), elongation at break (EB), modulus at 10 % elongation (M at 10 %) and at 100 % elongation (M at 100 %) for the CB-filled compounds and the AF-filled compounds in both the longitudinal and transverse directions and are displayed in Table 4. The TS for the AF-filled compounds were gradually increased in both the L and T direction as a function of fiber loading. However, the breaking elongations were gradually decreased and exhibited a brittle failure at 10 phr fiber loading. One of the probable reasons for this drastic reduction in the elongation at break might be due to the poor dispersion of the AF within the matrix. This in-homogeneously dispersed AFs may act as stress concentrated points under a tensile deformation leading to a sudden failure [25]. It is interesting

Table 4. Mechanical properties of the composites as a function of filler loadings

Composites with mill direction		Tensile strength (MPa)	Elongation at break (%)	10 % modulus (MPa)	100 % modulus (MPa)	300 % modulus (MPa)	Hardness (Shore-(A)
Neat		1.5±0.22	408±32	0.35±0.01	0.55±0.02	0.94±0.05	34±1
AF3	L	2.1±0.04	310±40	0.47±0.08	1.43±0.28	1.98±0.03	46±1
	T	2.1±0.06	246±45	0.78±0.19	1.94±0.16		
AF5	L	2.7±0.15	175±36	0.9±0.16	2.56±0.25		55±2
	T	2.6±0.09	211±39	1.0±0.07	2.57±0.12		
AF10	L	4.6±0.71	59±12	3.88±0.49			66±1
	T	5.6±0.47	62±12	2.86±0.61			
AF20	L	8.3±0.83	13±3	8.17±1.0			78±1
	T	6.6±0.38	51±10	5.12±0.77			
AF30	L	5.0±2.12	23±8	9.63±1.04			84±1
	T	8.8±1.51	22±9	7.71±1.44			
AF40	L	15.5±0.69	5.6±4				86±1
	T	11.7±1.73	25±6	10.72±2.35			
CB10		8.8±1.29	542±42	0.41±0.02	0.78±0.02	2.67±0.20	40±1
CB20		14.3±0.75	609±19	0.53±0.04	1.08±0.07	4.88±0.41	46±1
CB30		14.9±0.33	602±26	0.67±0.02	1.64±0.08	7.07±0.28	54±1
CB40		14.6±0.15	562±18	0.93±0.03	2.31±0.19	8.9±0.52	62±1

L indicates properties of the composite parallel to the mill direction; T indicates properties of the composite perpendicular to the mill direction.

to note that the low strain modulus: an indication of the stiffness of the composite significantly increased as the fiber content increased. For instance, the addition of just 3 phr AF enhanced the 10 % modulus by about 34 % in the L direction and further rose to about 1000 % with the addition of 10 phr AF. This dramatic increase in the low strain modulus shows a strong adhesion between the fiber and the matrix via polar interaction as shown in Scheme 1. In addition to this, at high fiber loading, some fibers can undergo certain degree of fibrillation during mixing as depicted in Figure 3. Due to fibrillation, the larger diameter fibers were split into thin fibrils having less than 2-3 micrometre in size [26]. As a result, the surface area of the fibers become increases which allow the fibers to interact more with the matrix. Moreover, the fibrillation creates certain surface roughness or corrugations on the fiber surface. This surface irregularity makes the fibers to tightly attach with the matrix via mechanical anchoring [25-27].

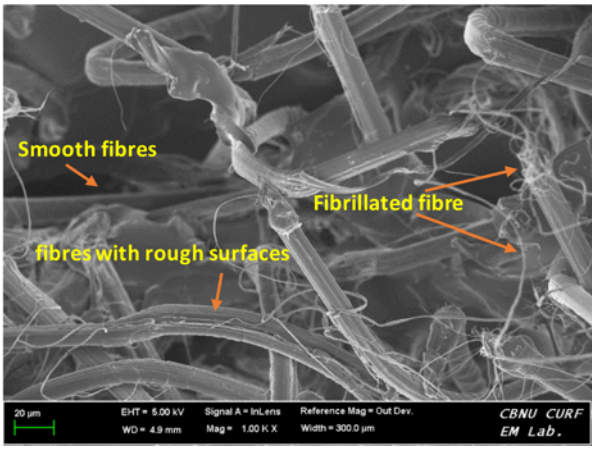

Figure 3. SEM photomicrographs of the tensile fracture surface of a 10 phr 1mm short aramid fiber-filled composite.

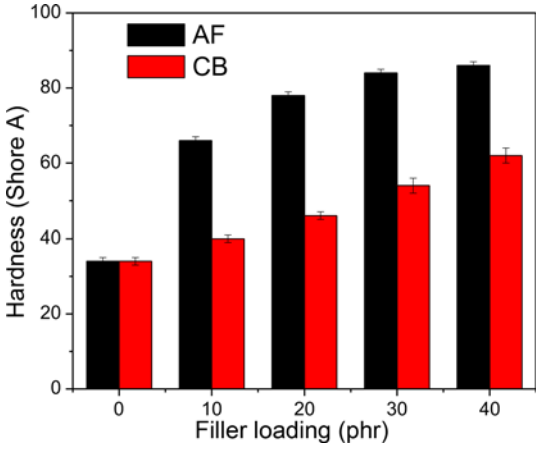

Figure 4. Shore-A hardness of the aramid fiber and the carbon black-filled composites as a function of filler loadings.

Depicted in Figure 4 is the hardness of the composites with fiber loading. It is well-known that hardness is a surface property which indicates the stiffness or brittleness of the materials. It can be seen from the figure that the hardness is significantly increased as the fiber content increased. For instance, with 3 phr of fiber loading, the hardness of the neat matrix was increased by 35 %. As the fiber content rose to 40 phr, the hardness was dramatically increased to 152 %.

The tensile deformation behaviors of CB-filled acrylic rubber was quite different than the fiber-filled one. The tensile strength of the neat matrix was increased by about 475 % with 10 phr addition of CB and further rose to 832 % with 20 phr CB and then level-off till the addition of 40 phr CB. At all CB loading, the composite showed remarkably higher elongation than the AF-filled one. This might be due to the uniform dispersion of the CB into the rubber matrix. However, at a given loading, the low strain modulus of the CB-filled composite was much lower than the AF-filled one. For instance, at 10 phr fiber loading, the 10 % modulus of the fiber-filled rubber was around 1000 % higher than those produced by CB-filled composite. The hardness of the CB-filled composites is also displayed in Figure 4. It is evident that at a given loading, the hardness of the black-filled compound was much lower than that of the fiber-filled composites.

Dynamic Mechanical Properties

Represented in Figures 5(a, b) are the storage modulus (E') and loss tangent (Tan δ) curves of short fiber and carbon black-filled acrylic rubber with different filler loading as a function of temperature. The viscoelastic properties obtained from the respective curves are displayed in Table 5. The storage moduli in the glassy (-40 ^{o}C) and rubbery (25 ^{o}C) regions for the AF-filled composites were larger than the neat matrix and are gradually increased as the fiber content increased. This enhancement in the storage moduli indicates the better interaction and reinforcing efficiency of the AFs with the acrylic rubber. From the values of storage moduli, the reinforcing effect of the AF with the acrylic rubber was calculated using the equation [28,29]

$$C = \frac{(E_g'/E_r')\ composite}{(E_g'/E_r')\ matrix} \quad (1)$$

where E_g' and E_r' are the storage modulus in the glassy region (at -40 ^{o}C) and rubbery regions (at 25 ^{o}C) respectively. In general, lower the C value higher will be the reinforcing effects of the filler as a reinforcing agent. The C values of the composite were decreased successively with fiber loading. This confirms that the reinforcement increased as the fiber content increased. The carbon black-filled acrylic rubber was also showed a similar trend in the storage modulus with loading. However, at a given loading, the E' of the CB-filled composite was much lower than the aramid fiber-filled one. For instance, at 10 phr loading, the E' of the

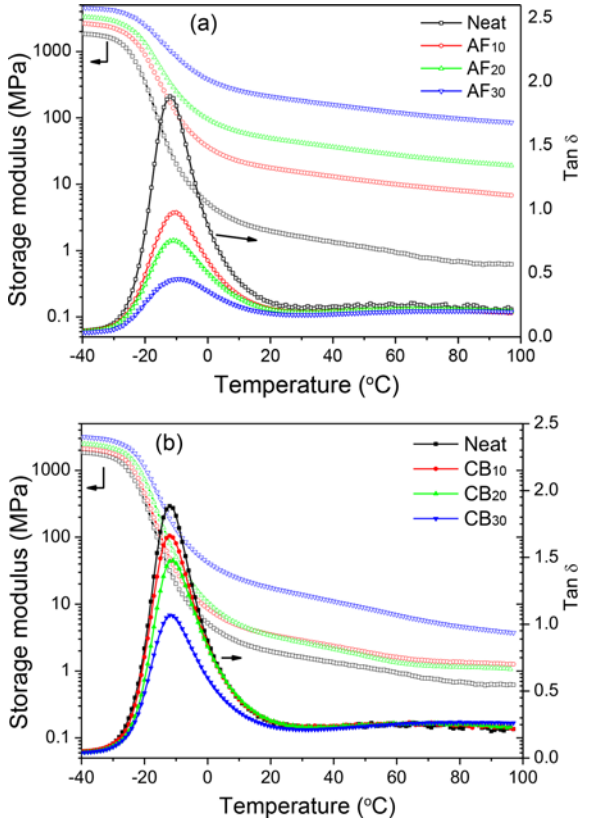

Figure 5. Storage modulus and tan delta curves as a function of temperature (a) short aramid fiber-filled composites in the L direction and (b) carbon black-filled composites at different filler loadings.

fiber-filled acrylic rubber at room temperature (25 °C) was around 823 % higher than the neat matrix. However, at the same loading, the E' of the CB-filled one was only 78 % higher than the neat matrix. This indicates that the ability of AF to reinforce the acrylic rubber was way better than the reinforcing efficiency of CB.

The effect of AF and CB loadings on the damping effects of their composites with acrylic rubber was also evaluated from their respective Tan δ versus temperature curves. The neat matrix showed a higher Tan δ peak with a Tan δ_{max} of 1.88 indicates the highest damping efficiency. However, the Tan δ peak height was decreased with fiber loading. At a 40 phr short fiber loading, the Tan δ_{max} was decreased from 1.88 to 0.45 with a peak shifting towards the higher temperature zone. This indicates that the addition of fibers decreased the damping effects due to the restricted movement of the polymeric chains by the reinforcing action of the fibers. On the other hand, at a given loading, the peak height of the Tan δ curve and the corresponding Tan δ_{max} of the CB-filled composite was higher than the AF-filled composite. For instance, at 10 phr loadings, the Tan δ_{max} of CB-filled composite was 1.66 and that of AF-filled composite was around 0.97. This means that the CB-filled composite can have better damping efficiency due to less restriction in the movements of the polymeric chains in its composites because of the poor reinforcement and weak filler-matrix interaction. From the values of Tan δ, the rubber-filler interaction was evaluated based on factor B as per the equation [25]

$$B = \frac{1-(\text{Tan }\delta_c/\text{Tan }\delta_m)}{V_f} \quad (2)$$

where B is the parameter which indicates the strength of the filler-matrix interfacial interaction, V is the volume fraction of the filler and the subscripts *f, m, c* denotes filler, matrix and composites respectively. In general, a high value of B indicates a strong fiber-matrix interfacial interaction. The values of B calculated using the above equation are displayed in Table 5. The 10 phr fiber-filled composite showed the highest B value and is decreased further as the content of short fiber increased. This was quite unexpected as per the theoretical prediction. One of the probable reasons for this might be due to the improper fiber dispersion in the matrix at a higher loading. However, the CB-filled compounds showed almost comparable values of B irrespective of the loadings. Here, it is worth noting that at a given loading, the B value of fiber-filled composite was higher than the black filled one. This confirms that the fiber-matrix interfacial adhesion

Table 5. Viscoelastic properties of the composites from the DMA analysis

Composite	E' at 40 °C (MPa)	E' at 25 °C (MPa)	E' at T_g (MPa)	Tan δ	T_g (°C)	C factor	B factor
Neat	1853	1.76	30.83	1.88	-11.86	1.00	
AF3	2206	5.17	59.76	1.48	-11.86	0.41	
AF5	2422	7.75	65.93	1.27	-10.70	0.30	
AF10	2644	16.28	142.32	0.98	-10.40	0.15	6.98
AF20	3328	45.25	293.89	0.76	-11.05	0.07	4.60
AF40	4587	196.0	812.12	0.45	-9.59	0.02	3.30
CB10	2113	2.98	42.43	1.67	-11.70	0.64	2.18
CB20	2494	3.15	70.12	1.48	-11.37	0.80	2.15
CB40	3180	15.61	182.29	1.07	-11.54	0.19	2.34

offered by the AF is much better than that offered by the CB.

Synergistic Effects of CB on the Properties of the Aramid Fiber-filled Rubber

From the stress-strain behavior and the corresponding tensile properties, it has been observed that the fiber-filled composite showed good stiffness (high 10 % modulus) but poor elongation at break (low toughness) compared to CB-filled composite. Therefore, a hybridization effect of CB and AF was practised to compromise the low elongation in AF-filled composite and the low modulus of the CB-filled composite. From the tensile properties, it has been observed that at 10 phr loading, the AF-filled composite showed a sudden declination in EB leading to poor toughness. However, the CB-filled composite showed an over-all good properties of TS and EB with excellent toughness at a loading of 20 phr. Therefore, we explored the reinforcing effect of a combination of 10 phr AF and 20 phr CB on to the acrylic rubber. Represented in Figure 6 are the stress-strain curves of 10 phr AF, 20 phr of CB and a combination of both 10 phr AF+20 phr CB-filled acrylic rubber. The properties such as TS, EB, 10 % modulus, shore-A hardness and compression set of the respective composites are displayed in Figures 7(a-d). Since the total filler content in the hybrid filler combination is 30 phr, for a comparative purpose, the properties offered by 30 phr AF and 30 phr CB were also included in the respective figures. The stress-strain curve of AF10+CB20 was almost close to AF10 in the low strain region. As the strain increased, it occupied a position in between AF10 and CB20 with an elongation of around 350 %, which was around 6 times higher than AF10. However, the 10 % modulus of the hybrid filler-filled composite in the L direction was almost comparable to AF10 and it was around 1145 % higher compared to CB20.

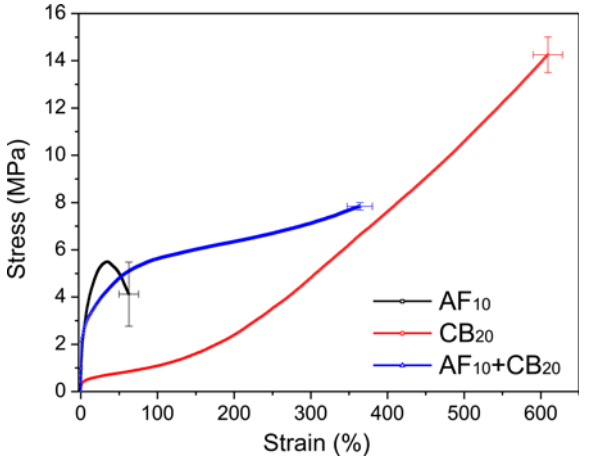

Figure 6. Stress-strain curves of AF10, CB-20 and a combination of AF10+CB20 in the L direction.

To figure out the enhanced stiffness and elongation observed in the hybrid filler-filled composite, SEM analysis was carried out on the tensile fractured surfaces. Represented in Figure 8(a, b) are the tensile fractured surfaces of AF10 and AF10+CB20 at a magnification of 10 kX. In both the composites, the fibers are in the process of pulling-out from

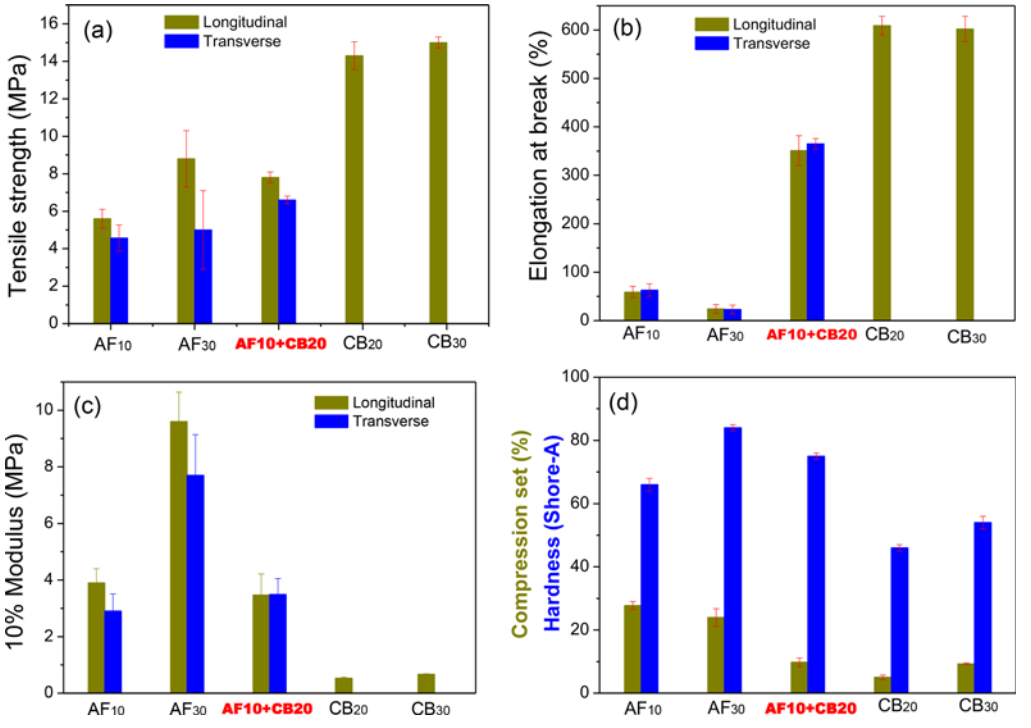

Figure 7. Tensile properties (a) TS, (b) EB, (c) 10 % modulus and (c) compression set and (d) hardness of the hybrid filler-filled composites.

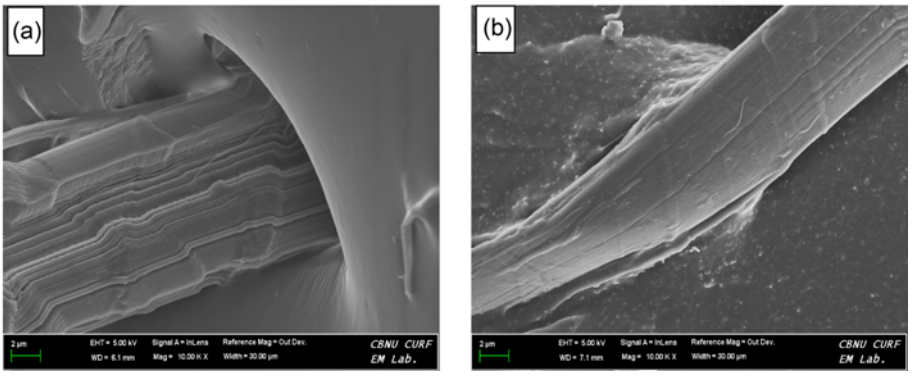

Figure 8. SEM photomicrographs of the tensile fractured surfaces of (a) AF10 and (b) AF10+CB20 at a magnification of 10 kX.

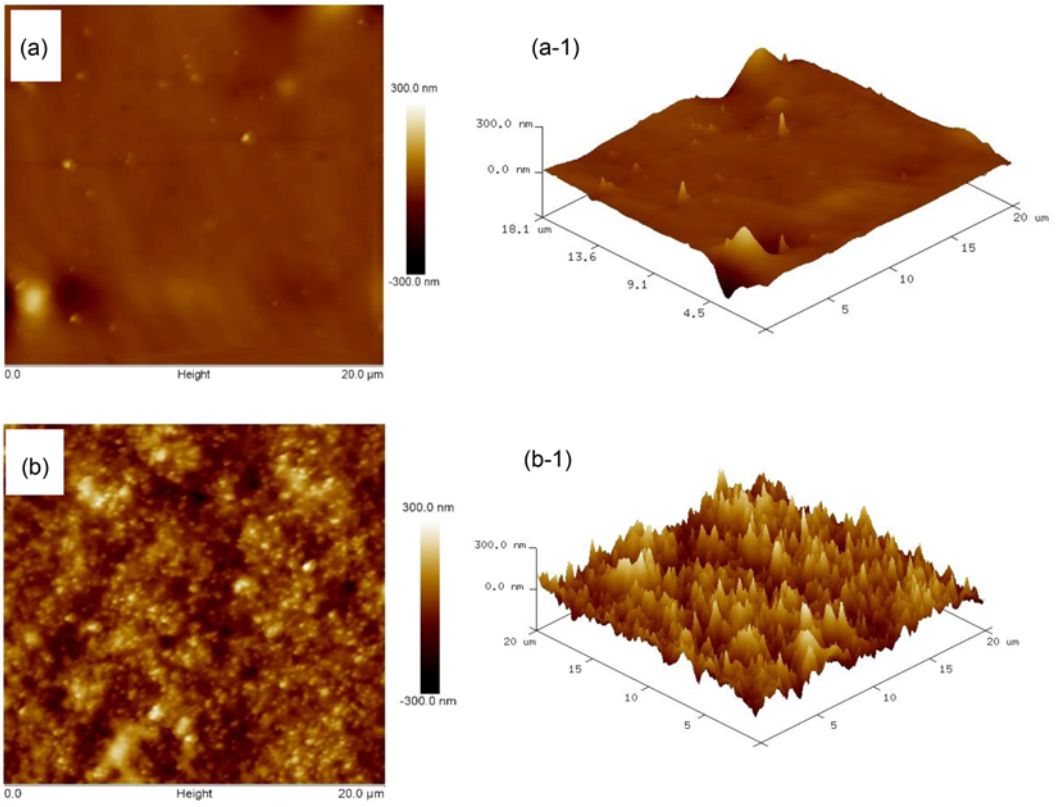

Figure 9. AFM surface topography of the smoothly cut surfaces of (a, a-1) AF10 and (b, b-1) AF10+CB20.

the matrix due to the tensile force. A fibrillated fiber with a smooth matrix surface can be seen in AF10. Here, the interface between the fiber and the matrix generate a de-bonding gap when the fiber is getting pulling-out from the matrix. This interface gap may enlarge at a strain greater than 60 % which eventually leads to brittle failure. On the other hand, a fiber with a rough matrix surface due to the presence of CB can be seen in the fracture surface of AF10+CB20. Moreover, here the matrix is firmly attached to the fiber and also elongated along with the fiber when it is getting pulling-out from the matrix. The surface morphology of these composites was also evaluated by AFM. Depicted in Figures 9(a, b) are the AFM images of the smoothly cut surfaces of AF10 and AF10+CB20 respectively. As seen in the SEM images, the AFM surface topography of AF10 was also smooth. Whereas, the AFM surface topography of AF10+CB20 was highly irregular due to the presence of uniformly distributed CB. From these morphological analyses, it is reasonable to believe that there may be a higher coefficient of friction at the interface between the CB-filled matrix and the fiber when the fiber is getting pulling-out from the matrix. As a result, the fiber pull-out

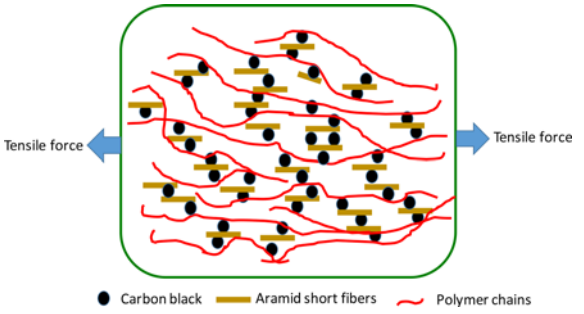

Scheme 2. Lubricating action of CB for the enhanced elongation (toughness) in the hybrid composite.

force will be higher and hence the modulus. Unlike AF10, the CB particle in AF10+CB20 can occupy in between the fibers and between the fibers and the polymer chains as depicted in Scheme 2. These entrapped CB particles can act as a lubricating agent and may enhance the slipping of the fibers one over another and also along the polymer chains at a higher tensile strain. This slipping mechanism can consume more tensile energy, as a result, the composite AF10+CB20 exhibits higher elongation with improved toughness.

The effects of hybridization on the dynamic mechanical properties were also studied. Represented in Figure 10 are the E' and tan delta curves of the hybrid composites as a function of temperature. For a comparative evaluation, the E' and tan delta curves of AF10 and CB20 are also included in the figure. The hybrid filler-filled composite showed a higher E' value compared to AF10 or CB20 at 25 °C. Moreover, the tan delta peak height of the hybrid filler-filled composite was lower than AF10 and CB20 indicating the better reinforcing performance of the hybrid filler. It is interesting to note that incorporation of 20 phr CB onto 10 phr AF-filled composites shifted its Tg from -10.4 °C to -11.7 °C. This low-temperature shifting of the glass transition temperature indicates the enhanced flexibility or movements

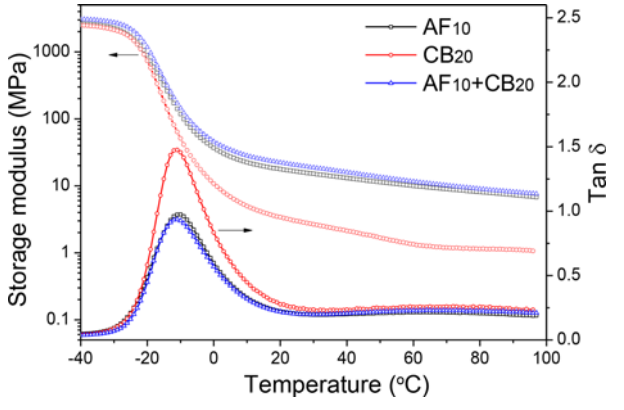

Figure 10. Storage modulus and tan delta curves of AF10, CB20 and its hybrid composites as a function of temperature.

of the polymeric chains in AF10+CB20 due to the lubricating or the plasticizing action of CB depicted in Scheme 2.

Effect of Fiber Length on the Hybridization

It is well-known that incorporation of high length fibers can impart better mechanical properties particularly, the strength and stiffness at a relatively low fiber loading. However, the successful dispersion of high length fibers into the polymer matrix is very difficult due to the severe fiber entanglement during shear mixing [29]. Represented in Figures 11(a-c) and Table 6 are the stress-strain behavior and the corresponding tensile properties of 1, 3 and 5 mm short AFs at 5 phr loading. The 1mm short-fiber-filled composite offered a 10 % modulus of 0.9 MPa with a breaking elongation of 175 % in the longitudinal direction. However, both the 3 mm and 5 mm fiber-filled composite showed a brittle failure even at a 5 phr loading with a breaking elongation of 78 % and 33 % respectively. But, the 10 % moduli of a 5 phr 3 mm and 5 mm fiber-filled composite were 127 % and 367 % higher than the 1mm fiber-filled composites. Severe fiber entanglement and fiber aggregation were identified as one of the major reasons behind the brittle failure in both the 3 mm and 5 mm fiber-filled composites. To solve this problem, 20 phr CB was incorporated along with 5 phr AF. The resultant stress-strain behavior and the tensile properties are also displayed in Figures 11(a-c) and

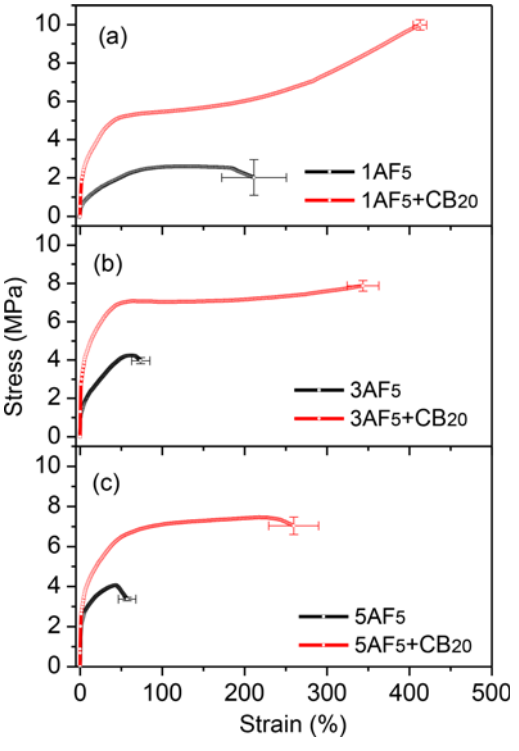

Figure 11. Stress-strain curves of 5 phr AF and a combination 5 phr AF with 20 phr CB having different fiber lengths (a) 1 mm, (b) 3 mm, and (c) 5 mm.

Table 6. Mechanical properties of the hybrid composites having different of fiber length

Composites with mill direction		Tensile strength (MPa)	Elongation at break (%)	10 % modulus (MPa)	100 % modulus (MPa)	300 % modulus (MPa)	Hardness (Shore-A)
1 mm AF5	L	2.7±0.15	175±36	0.9±0.16	2.56±0.25	-	55±2
	T	2.6±0.09	211±39	1.0±0.07	2.57±0.12	-	
1 mm AF5+CB20	L	10.0±0.27	412±8	3.40±0.26	5.45±0.30	7.42±0.25	67±1
	T	10.4±0.34	443±10	1.32±0.10	3.75±0.18	7.34±0.07	
3 mm AF5	L	4.0±0.08	78±8	2.05±0.21	-	-	54±1
	T	3.4±0.09	128±8	1.78±0.10	3.61±0.12	-	
3 mm AF5+CB20	L	8.1±0.03	354±5	4.82±0.05	7.15±0.12	7.66±0.06	68±1
	T	10.1±0.14	456±17	2.00±0.29	4.04±0.27	7.18±0.21	
5 mm AF5	L	2.9±0.12	33±12	4.21±0.66	-	-	54±2
	T	2.9±0.21	86±17	1.80±0.11	-	-	
5 mm AF5+CB20	L	7.3±0.17	233±9	4.25±0.12	7.03±0.27	-	62±1
	T	8.5±0.44	402±22	1.50±0.06	4.16±0.08	7.16±0.14	

L indicates properties of the composite parallel to the mill direction; T indicates properties of the composite perpendicular to the mill direction.

Table 6. Interestingly, TS, EB, 10 % modulus and hardness of all the hybrid composites were remarkably better than the composite with either AF alone or CB alone. This property enhancement clearly confirms that the carbon black can act as toughening as well as a stiffening agent in conjunction with the aramid fiber.

Thermogravimetric Analysis

Represented in Figures 12(a, b) are the weight loss and the corresponding derivative thermogram (DTG) for the neat CB powder, neat aramid fiber, neat vulcanized matrix and their composites with 30 phr AF (AF 30) and 30 phr CB (CB-30) as a function of temperature. Here, the composites with 30 phr AF and 30 phr CB were taken for a comparative analysis of its thermal properties with the hybrid composites, which has also a total filler content of 30 phr. The CB powder shows no significant weight-loss and hence shows no thermal degradation peak. However, the AF exhibit an onset of thermal degradation ($T_{i5\%}$) at a temperature of 369 °C with a maximum degradation peak (T_{max}) at 573 °C. The neat vulcanized matrix also showed an onset of thermal degradation temperature around 369 °C, but exhibit a T_{max} at 439 °C. The $T_{i5\%}$ and T_{max} of a 30 phr AF-filled composite were more or less similar to that of the neat vulcanized matrix. This indicates that the addition of AF does not significantly improved the thermal properties of the matrix. However, the onset of thermal degradation temperatures for the 30 phr CB-filled composite and the hybrid filler-filled composite was shifted to a higher temperature zone by 21-22 °C with a T_{max} of 443-445 °C. This indicates that the addition of CB remarkably improved the thermal stability of the composite due to its inherent high-temperature degradation characteristics. It is interesting to note that both the composite,

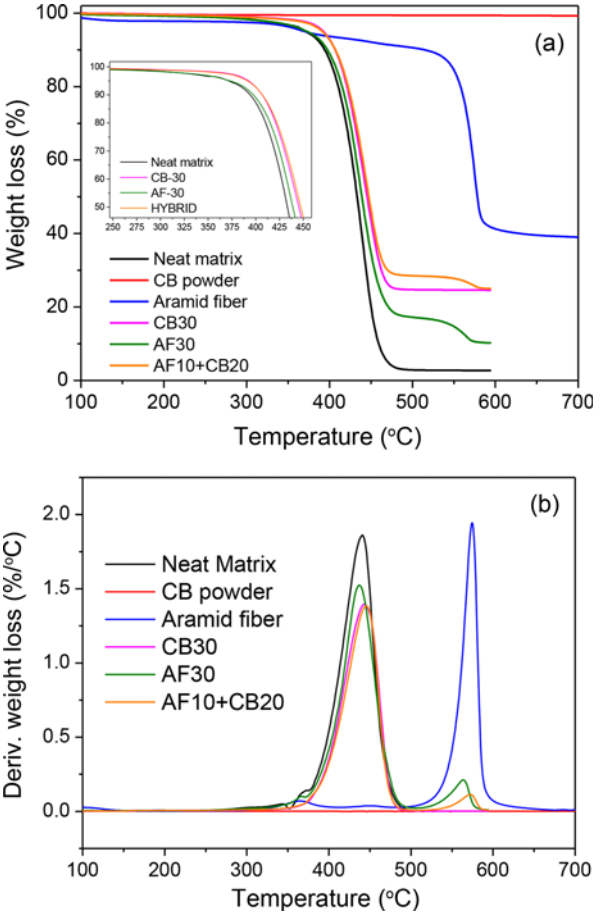

Figure 12. (a) TGA and (b) DTG curves of neat matrix, neat CB powder, neat AF, composites with 30 phr CB, 30 phr AF and a combination of 10 phr AF+ 20 phr CB.

AF30 and AF10+CB20 exhibits two peak maxima in their derivative curves. Here, the major peak appeared in the range of 443-445 ^{o}C is responsible for the matrix degradation and the minor peak appeared in the range of 564-569 ^{o}C is probably due to the degradation of the AFs present in the composites.

Conclusion

The reinforcing effects of 1mm short aramid fiber and carbon black on the stress-strain behavior and the mechanical properties of an ethylene-acrylic rubber were analysed as a function of filler loading. The fiber-filled composite showed good low-strain modulus (stiffness) but, poor breaking elongation (toughness) as the filler loading increased. On the other hand, the CB-filled composite exhibited a high breaking elongation with poor low-strain modulus or stiffness. On reinforcing the acrylic rubber with a combination of 10 phr AF and 20 phr CB exhibited a synergistic effect. As a result, the poor TS and breaking elongation of the fiber-filled composites and the inferior low-strain modulus of the CB alone filled composites could be greatly compromised. From the dynamic mechanical analysis, it has been observed that the addition of 20 phr CB shifted the glass-transition temperature of the 10 phr fiber-filled composite to a lower temperature region. This indicated that the flexibility of the 10 hr aramid fiber-filled composites considerably increased by the addition of 20 phr CB onto it. From the tensile fractured surface analysis of the hybrid filler-filled composite, it has been assumed that the CB which are entrapped between the fibers and between the fiber and the polymer chains can acts as stiffening agent as well as toughening agent. The stiffening action is mainly originated from the coefficient of friction between the fiber and the CB. However, the toughening action is originated from the lubricating action of the CB which are entrapped in between the fibers and the polymer chains.

Acknowledgement

This work was supported by the Basic Science Research Program through the National Research Foundation of Korea (NRF) funded by the Ministry of Education (NRF-2016R1D1A3B03932709).

References

1. S. K. De and J. R. White, “Short Fiber Polymer Composites”, Woodhead, Cambridge, England, 1996.
2. M. J. Folkes, “Short Fiber Reinforced Thermoplastics”, John Wiley and Sons Ltd., 1982.
3. D. C. Derringer, *J. Elastoplast.,* **3**, 230 (1971).
4. L. A. Goettler and K. S. Shen, *Rubb. Chem. Technol.,* **56**, 619 (1983).
5. L. A. Goettler and K. S. Shen, *Polym. Comp.,* **5**, 60 (1984).
6. J. E. O’Connor, *Rubb. Chem. Technol.,* **50**, 945 (1977).
7. W. B. Wennekes, J. W. M. Noordermeer, and R. N. Datta, *Kautsch Gummi Kunstst.,* **60**, 20 (2007).
8. W. B. Wennekes, J. W. M. Noordermeer, and R. N. Datta, *Rubb. Chem. Technol.,* **80**, 545 (2007).
9. W. B. Wennekes, J. W. M. Noordermeer, and R. N. Datta, *Rubber Chem. Technol*., **80**, 565 (2007).
10. S. Praveen, P. K. Chattopadhyay, S. Jayendran, B. K. Chakraborty, and S. Chattopadhyay, *Polym. Int.,* **59**, 187 (2010).
11. M. Shirazi and J. W. M. Noordermeer, *Rubber Chem. Technol*., **84**, 187 (2011).
12. M. Shirazi, A. G. Talma, and J. W. M. Noordermeer, *J. Adhes. Sci. Technol.,* **27**, 1048 (2013).
13. M. Shirazi, A. G. Talma, and J. W. M. Noordermeer, *J. Appl. Polym. Sci*., **128**, 2255 (2013).
14. C. Hintze, M. Shirazi, S. Wiessner, A. G. Talma, G. Heinrich, and J. W. M. Noordermeer, *Rubber Chem. Technol*., **86**, 579 (2013).
15. C. Hintze, C. R. Boldt, S. wiessner, G. Heinrich, and J. W. M. Noordermeer, *J. Appl. Polym. Sci*., **130**, 1682 (2013).
16. P. Pittayavinaim, S. Thanawan, and T. Amornsakchai, *Polym. Test*., **64**, 109 (2017).
17. B. Zhang, B. Gu, and X. Yu, *J. Appl. Polym. Sci.,* **132**, 41672 (2015).
18. M. Tian, L. Su, W. Cai, S. Yin, Q. Chen, H. Fong, and L. Zhang, *J. Appl. Polym. Sci*., **120**, 1439 (2011).
19. H. S. Mohammed, K. Elangovan, and V. Subrahmanian, *Indian J. Adv. Chem. Sci.*, **4**, 458 (2016).
20. B. C. Begnoche, R. L. Keefe, and A. G. Causa, *Rubber Chem. Technol.,* **60**, 689 (1987).
21. X. He, X. Shi, M. Hoch, and C. Gogelein, *Polym. Compos.,* **39**, 3212 (2017).
22. M. R. Kashani, *J. Appl. Polym. Sci*., **113**, 1355 (2009).
23. N. Kanbargi and A. J. Lesser, *J. Appl. Polym. Sci*., doi:10.1002/APP.45520 (2017).
24. K. Gerard, *Macromol. Mater. Eng*., **60**, 215 (1977).
25. S. Gopi Sathi, H. Kim, Y. Seong, G. Kang, and C. Nah, *Polym. Compos.*, doi:10.1002/pc.25141 (2018).
26. S. Gopi Sathi and K. Naskar, *J. Appl. Polym. Sci*., **130**, 2205 (2013).
27. S. Gopi Sathi, J. Jeon, H. H. Kim, and C. Nah, *Plast. Rubber Compos*., **48**, 115 (2019).
28. S. Gopi Sathi and K. Naskar, *Polym. Compos*., **35**, 1767 (2014).
29. S. Gopi Sathi and K. Naskar, *Express Polym. Lett.,* **6**, 329 (2012).